

Spin Separation in Cyclotron Motion

L. P. Rokhinson* and V. Larkina

Department of Physics, Purdue University, West Lafayette, Indiana 47907, USA

Y. B. Lyanda-Geller

Naval Research Laboratory, Washington, D.C. 20375, USA

L. N. Pfeiffer and K. W. West

Bell Laboratories, Lucent Technologies, Murray Hill, New Jersey 07974, USA

(Received 8 July 2004; published 28 September 2004)

Charged carriers with different spin states are spatially separated in a two-dimensional hole gas. Because of strong spin-orbit interaction, holes at the Fermi energy in GaAs have different momenta for two possible spin states traveling in the same direction, and, correspondingly, different cyclotron orbits in a weak magnetic field. Two point contacts, acting as a monochromatic source of ballistic holes and a narrow detector arranged in the magnetic focusing geometry are demonstrated to work as a tunable spin filter.

DOI: 10.1103/PhysRevLett.93.146601

PACS numbers: 72.25.-b, 71.70.Ej, 73.23.Ad, 85.75.-d

The ability to manipulate the spin of charge carriers in a controllable fashion is a central issue in the rapidly developing field of spintronics [1], as well as in the development of spin-based devices for quantum information processing [2]. Electrical injection of spin-polarized currents has proven to be a formidable challenge. To date, spin-polarized currents have been generated either by using ferromagnetic materials as injectors [3–6] or by exploiting the large spin splitting of electron energy levels in strong magnetic fields [7,8]. Here we realize a solid-state analog of the Stern-Gerlach experiment in atomic physics [9], with spin-orbit interactions playing the role of the gradient of magnetic field. We achieve spatial separation of spins and bipolar spin filtering using cyclotron motion in a weak magnetic field.

Our approach is to use intrinsic spin-orbit (SO) interactions existing in low-dimensional systems. It has long been appreciated that such interactions can be interpreted as an effective momentum-dependent magnetic field that influences spin of charge carriers [10]. More recently, it has been recognized [11–14] that SO interactions can also be viewed as an effective orbital magnetic field with an opposite sign for different spin orientations. Now, assume that two different magnetic fields $B_{\pm} = B_{\perp} \pm B_{so}$ affect the orbital motion of charge carriers with two distinct spins. Here, B_{\perp} is the perpendicular external magnetic field and B_{so} is the spin-orbital effective field characteristic for cyclotron motion. Then, charge carriers move along the cyclotron orbit with spin-dependent radius $R_c^{\pm} = p_f/e(B_{\perp} \pm B_{so})$, where $p_f = \sqrt{2m\epsilon_f}$ and ϵ_f are the Fermi momentum and energy, and e is the charge of carriers. A spin-dependent R_c has been observed in commensurability oscillations [15]. Our goal here is to use the spin dependence of R_c for spatial separation of carriers

with distinct spins. To do this, we use magnetic focusing [16–18] that we show to be spin dependent as a result of SO interactions. In the magnetic focusing configuration, charge carriers are injected in the two-dimensional gas through the injector quantum point contact (QPC), propagate along the orbits defined by R_c^{\pm} , and are detected by the detector QPC. By adjusting R_c , we select the spin of charge carriers that reach the detector. Tuning R_c is possible by either changing B_{\perp} , changing electron density with electrostatic gates ($p_f^2 = 2\pi\hbar^2 n$, where n is the carrier density), or changing B_{so} by adjusting the external electric fields [19,20].

To demonstrate spatial separation of spins experimentally we fabricated several devices in the magnetic focusing geometry from two-dimensional hole gas (2DHG); see inset of Fig. 1. The structure is formed using the atomic force microscopy (AFM) local anodic oxidation technique [21–23]. Oxide lines separate the 2DHG underneath by forming ~ 200 mV potential barriers. A specially designed heterostructure is grown by molecular-beam epitaxy on [113]A GaAs. Despite very close proximity to the surface (350 Å), the 2DHG has an exceptionally high mobility 0.4×10^6 V s/cm² and relatively low hole density $n = 1.38 \times 10^{11}$ cm⁻². The device consists of two QPCs separated by a central gate. Potential in the point contacts can be controlled separately by two gates G_{inj} and G_{det} , or by the central gate G_c . In our experiments the central gate was kept at -0.3 V, and ~ 0.2 V were applied to the gates G_{inj} and G_{det} . Asymmetric biasing of point contacts provides sharper confining potential and reduces the distance between the two potential minima by $\Delta L \sim 0.07$ μm.

Magnetic focusing manifests itself as equidistant peaks in magnetoresistance $R(B_{\perp})$ for only one direction

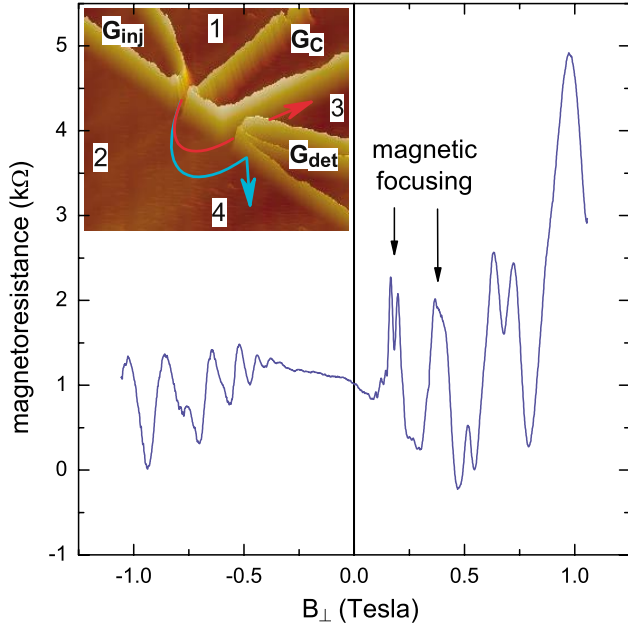


FIG. 1 (color online). Magnetoresistance and layout of focusing devices. Voltage across the detector (contacts 3 and 4) is measured as a function of magnetic field perpendicular to the surface of the sample (B_{\perp}). Lithographical separation between point contacts is $0.8 \mu\text{m}$. Current of 1 nA is flowing through the injector (contacts 1 and 2). Positions of the magnetic focusing peaks are marked with arrows. Inset: AFM micrograph of a sample ($5 \mu\text{m} \times 5 \mu\text{m}$). Light lines are the oxide which separates different regions of 2D hole gas. Conductance of quantum point contacts is controlled via voltages applied to the detector G_{det} , injector G_{inj} and the central G_C gates. Semicircles show schematically the trajectories for two spin orientations.

of B_{\perp} . R is measured by applying a small current through the injector QPC while monitoring voltage across the detector QPC; see inset of Fig. 1. At $B_{\perp} < 0$ cyclotron motion forces carriers away from the detector. Then, only 2DHG contributes to R , which has almost no B_{\perp} dependence at low fields and shows Shubnikov–de Haas oscillations at $|B_{\perp}| > 0.3$ T. For $B_{\perp} > 0$ several peaks due to magnetic focusing are observed. Peaks' separation $\Delta B \approx 0.18$ T is consistent with the expected value for the lithographical distance between the injector and detector QPCs $L = 0.8 \mu\text{m}$. The data are symmetric upon the exchange of the injector and detector and simultaneous reversal of the magnetic field direction.

The first focusing peak is a doublet consisting of two peaks separated by 36 mT. These peaks are the sharpest when both QPCs are gated to pass exactly one spin-degenerate mode [within the $G = 2e^2/h = 12.9$ kΩ conductance plateau in the QPC characteristic, Fig. 2(b)]. Peaks in a doublet have approximately the same height.

A QPC can be used as a spin filter for one spin polarization if spin degeneracy is lifted by Zeeman splitting of energy levels in a strong magnetic field [24]. We apply an

in-plane field B_{\parallel} , which has little effect on the cyclotron motion of holes but acts on their spin degrees of freedom. At $B_{\parallel} = 3.3$ T there is a pronounced step at e^2/h in conductance vs gate voltage characteristic in both QPCs; see Fig. 2(b). The appearance of this step means that Zeeman energy exceeds both the broadening of the transverse quantized energy levels of the QPC and the temperature. Then, for $G \leq e^2/h$ only holes with one spin polarization are allowed to pass through the point contact. Experiments [24] with electrons had shown reduction of the height of the focusing peaks by 50% due to spin filtering, when conductance of one QPC was tuned below e^2/h and conductance of the other QPC was maintained at $2e^2/h$.

We use the spin filtering by QPCs at high B_{\parallel} to probe the spin states which correspond to the first focusing peak doublet. As the conductance of the injector QPC is reduced below $2e^2/h$, the height of the high-field peak in the doublet reduces while the height of the low-field peak remains almost the same; see Figs. 2(c) and 2(d). When conductance of the injector QPC is $\sim 0.5e^2/h$, the high-field peak almost vanishes in a striking contrast to the electron case. Similarly, the high-field peak vanishes if the detector acts as a spin filter while the injector is tuned to accept both spin polarizations. In contrast, at zero B_{\parallel} peak relative strength does not change significantly as the injector conductance is decreased; see Fig. 2(a). A small suppression of the high-field peak at B_{\parallel} can be attributed to a partial lifting of the spin degeneracy in a nonzero focusing field $B_{\perp} = 0.2$ T. Therefore, we conclude that the two peaks within the doublet correspond to the two spin states of the holes. The peak spacing of 36 mT means that focusing points for the two spin states are ≈ 120 nm apart.

In order to explain the effect qualitatively, we assume that charge carriers in the GaAs quantum well are characterized by the isotropic kinetic energy and the Dresselhaus spin-orbit interaction, so that the Hamiltonian can be written as [25] $H = \frac{1}{2m}(p_x + \gamma\sigma_x)^2 + \frac{1}{2m}(p_y - \gamma\sigma_y)^2$, where m is the effective mass, \vec{p} is the electron momentum, σ_i are the Pauli matrices ($i = x, y$), and γ is the spin-orbit parameter. For simplicity, we neglect anisotropy of the effective mass that does not change the qualitative picture. In the semiclassical description, appropriate for the range of magnetic fields B_{\perp} used for the focusing, the motion is described by simple equations

$$\begin{aligned} \frac{d\vec{p}}{dt} &= e\vec{v} \times \vec{B}, & \vec{v} &= \frac{d\vec{r}}{dt} = \frac{\partial \epsilon_{\pm}(\vec{p})}{\partial \vec{p}}, \\ \epsilon_{\pm} &= \frac{1}{2m}(p \pm \gamma)^2 + \frac{\gamma^2}{2m}, \end{aligned} \quad (1)$$

where \vec{r} , \vec{v} , and ϵ_{\pm} are the charge carrier coordinate, velocity, and energy for the two spin projections. This description implies that the carrier wavelength is

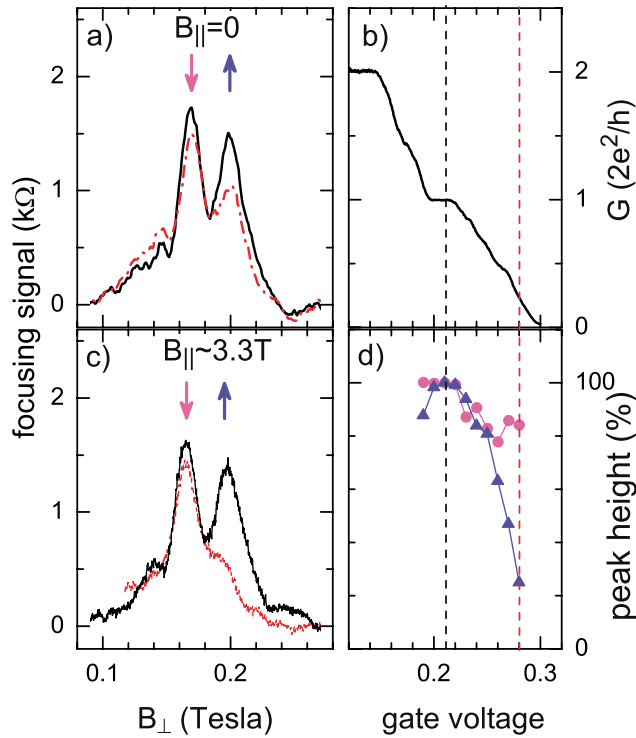


FIG. 2 (color online). Magnetoresistance is measured with magnetic field oriented (a) perpendicular or (c) at $\sim 3^\circ$ to the surface. Series resistance due to 2DHG is subtracted. In-plane field $B_{\parallel} = 3.3$ T corresponds to the center of the peak and is aligned with the direction of the carriers injection. Black (solid) curves are measured with injector and detector QPCs gated to pass both spin orientations (conductance $G = 2e^2/h$). Red (dashed) curves are measured with injector QPC gated at $G \approx 0.5e^2/h$. In (b) conductance of the injector QPC is plotted as a function of the gate voltage at $B_{\parallel} = 3.3$ T. (d) Height of the low- (magenta dots) and high-field (blue triangles) peaks in (b) is plotted as a function of the injector gate voltage.

smaller than the cyclotron radius, and that jumps between orbits with different spin projections are absent, i.e., $\epsilon_f \gg \gamma p/m \gg \hbar\omega_c$. Equations (1) show that the charge carrier with energy $\epsilon_{\pm} = \epsilon_f$ is characterized by the spin-dependent trajectory: momentum \vec{p}_{\pm} , coordinate \vec{r}_{\pm} , and cyclotron frequency ω_c^{\pm} . The solution to these equations is

$$\begin{aligned} p_{\pm}^{(x)} + ip_{\pm}^{(y)} &= p_{\pm} \exp(-i\omega_c^{\pm} t), \\ r_{\pm}^{(x)} + ir_{\pm}^{(y)} &= \frac{i\sqrt{2m\epsilon_f}}{m\omega_c^{\pm}} \exp(-i\omega_c^{\pm} t), \\ \omega_c^{\pm} &= \frac{eB_{\perp}}{m} (1 \pm \gamma/p_{\pm}). \end{aligned} \quad (2)$$

Thus, as discussed in the introduction, the cyclotron motion is characterized by the spin-dependent field $B_{\pm} = B_{\perp}(1 \pm \gamma/p_{\pm})$. Using the semiclassical limit of the quantum description, one obtains the identical results [26].

In the focusing configuration QPCs are used as monochromatic point sources. Holes, injected in the direction perpendicular to the two-dimensional hole gas boundary, can reach the detector directly or after specular reflections from the boundary. As follows from Eqs. (2), for each of the two spin projections there is a characteristic magnetic field such that the point contact separation is twice the cyclotron radius for a given spin, $L = 2R_{\pm}^c = 2p_f/eB_{\pm}$, $p_f = \sqrt{2m\epsilon_f}$. The first focusing peak occurs at

$$B_{\perp}^{\pm} = \frac{2(p_f \mp \gamma)}{eL}. \quad (3)$$

The magnitude of γ can be calculated directly from the peak splitting $\gamma = (B_{\perp}^+ - B_{\perp}^-)eL/4 = 7 \times 10^{-9}$ eV s/m. A larger value of $\gamma \approx 25 \times 10^{-9}$ eV s/m was extracted from the splitting of cyclotron resonance at 3 times higher hole concentration [27]. For electrons, a much smaller value $\gamma \approx 1.5 \times 10^{-9}$ eV s/m characterizes the combined spin-cyclotron resonance [28]. We note that Eq. (3) is more general than Eqs. (2). The coefficient γ essentially describes the separation in momentum space of the two parts of the Fermi surface which correspond to $\epsilon^{\pm} = \epsilon_f$, and includes contributions of various spin-orbit terms in the 2D hole gas. Analysis of the second and higher focusing peaks is complicated by the mixing of spin states due to reflections from the boundary. If carriers necessarily undergo transitions between ϵ^+ and ϵ^- parts of the Fermi surface upon reflections, no splitting of the second and other even focusing peaks is expected [29].

We now discuss spin states and their filtering by QPCs in more detail. In the presence of SO interactions carriers are characterized by the projection of their spin on the total magnetic field, which is composed of the external magnetic field and the effective momentum-dependent SO field. In our devices, the characteristic energy of SO interactions $\gamma p_f/m \approx 0.2$ meV is larger than the Zeeman energy, and the quantum states of the 2D holes are well characterized by the sign of the spin projection onto their momentum \vec{p} ($g^* \mu_B B \approx 0.08$ meV at 3.5 T, $g^* \approx 0.4$ for [233] crystallographic direction). R_c for these 2D states are different for different spin projection signs.

However, in a QPC the hole momentum decreases and even vanishes on the plateau, so that $\gamma p/m < g^* \mu_B B$. In this case holes are characterized by their spin projection on the external magnetic field. Thus, they can be spin filtered by gating the QPC to $G < e^2/h$. A hole, leaving injector in a certain spin state, enters the detector with the same spin orientation as long as the 1D spin states in both QPCs adiabatically evolve into \vec{p} -projection states in the 2DHG, and spin evolution is adiabatic along the ballistic cyclotron trajectory.

The spin-dependent focusing field B_{\perp}^{\pm} is proportional to the spin-orbit constant γ and does not depend on the cyclotron frequency $\omega_c = eB_{\perp}/m$. At the same time, the spin-dependent cyclotron frequency in Eq. (2) is proportional to both ω_c and γ . Thus, the effective magnetic field B_{so} is itself proportional to B_{\perp} . This effect differs from the spin-dependent shift of the Aharonov-Bohm oscillations in the conductance of rings, where the additional spin-orbit flux and the Aharonov-Bohm flux are independent of each other [11]. If the Zeeman effect is taken into account, both ω_c^{\pm} and R_c^{\pm} acquire additional dependence on B_{\perp} , as well as on B_{\parallel} . However, in the present experimental setting the Zeeman splitting is small compared to the effects of SO interactions and is essential for filtering spins in the injector and detector QPCs only.

The phenomenon we report in this Letter is not restricted to holes in GaAs but is generic to any system with intrinsic spin-orbit interactions. We believe that exceptional quality two-dimensional hole systems provide novel opportunities for spin manipulation. In particular, it will be possible to realize other schemes of spin separation and filtering [30,31].

In conclusion, we developed a method to spatially separate spin currents in materials with intrinsic spin-orbit interactions by a weak magnetic field. This has been achieved in semiclassical cyclotron motion, where distinct spins are characterized by distinct cyclotron radii and frequencies. Thus the cyclotron motion can separate not only the particles with different masses but also particles with different spin-orbit parameters. We confirm the spatial separation of spins experimentally by selectively detecting spin-polarized currents.

The authors thank A. M. Finkelstein and G. F. Giuliani for enlightening discussion. The work was partially funded by DARPA and NSA/ARDA.

*Electronic address: leonid@physics.purdue.edu

- [1] S. A. Wolf, D. D. Awschalom, R. A. Buhrman, J. M. Daughton, S. V. Molnar, M. L. Roukes, A. Y. Chtchelkanova, and D. M. Treger, *Science* **294**, 1488 (2001).
- [2] P. D. DiVincenzo, *Science* **270**, 255 (1995).
- [3] R. Fiederling, M. Keim, G. Reuscher, W. Ossau, G. Schmidt, A. Waag, and L. W. Molenkamp, *Nature (London)* **402**, 787 (1999).
- [4] Y. Ohno, D. K. Young, B. Beschoten, F. Matsukura, H. Ohno, and D. D. Awschalom, *Nature (London)* **402**, 790 (1999).
- [5] F. J. Jedema, H. B. Heersche, A. T. Filip, J. J. A. Baselmans, and B. J. V. Wees, *Nature (London)* **416**, 713 (2002).
- [6] P. R. Hammar and M. Johnson, *Phys. Rev. Lett.* **88**, 066806 (2002).
- [7] J. A. Folk, R. M. Potok, C. M. Marcus, and V. Umansky, *Science* **299**, 679 (2003).
- [8] R. Hanson, B. Witkamp, L. M. K. Vandersypen, L. H. W. V. Beveren, J. M. Elzerman, and L. P. Kouwenhoven, *Phys. Rev. Lett.* **91**, 196802 (2003).
- [9] W. Gerlach and O. Stern, *Z. Phys.* **9**, 349 (1922).
- [10] E. I. Rashba, *Sov. Phys. Solid State* **2**, 1109 (1960).
- [11] A. G. Aronov and Y. B. Lyanda-Geller, *Phys. Rev. Lett.* **70**, 343 (1993).
- [12] D. Loss, P. Goldbart, and A. V. Balatsky, *Phys. Rev. Lett.* **65**, 1655 (1990).
- [13] Y. Aharonov and A. Casher, *Phys. Rev. Lett.* **53**, 319 (1984).
- [14] I. L. Aleiner and V. I. Fal'ko, *Phys. Rev. Lett.* **87**, 256801 (2001).
- [15] J. P. Lu, J. B. Yau, S. P. Shukla, M. Shayegan, L. Wissinger, U. Rössler, and R. Winkler, *Phys. Rev. Lett.* **81**, 1282 (1998).
- [16] Y. V. Sharvin, *Zh. Eksp. Teor. Fiz.* **48**, 984 (1965) [*Sov. Phys. JETP* **21**, 655 (1965)].
- [17] V. S. Tsoi, *JETP Lett.* **22**, 197 (1975).
- [18] H. vanHouten, C. W. J. Beenakker, J. G. Williamson, M. E. I. Broekaart, P. H. M. vanLoosdrecht, B. J. vanWees, J. E. Mooij, C. T. Foxon, and J. J. Harris, *Phys. Rev. B* **39**, 8556 (1989).
- [19] J. B. Miller, D. M. Zumbuhl, C. M. Marcus, Y. B. Lyanda-Geller, D. Goldhaber-Gordon, K. Campman, and A. C. Gossard, *Phys. Rev. Lett.* **90**, 076807 (2002).
- [20] S. J. Papadakis, E. P. DePoortere, H. C. Manoharan, J. B. Yau, M. Shayegan, and S. A. Lyon, *Phys. Rev. B* **65**, 245312 (2002).
- [21] E. S. Snow and P. M. Campbell, *Appl. Phys. Lett.* **64**, 1932 (1994).
- [22] R. Held, T. Heinzel, A. P. Studerus, K. Ensslin, and M. Holland, *Appl. Phys. Lett.* **71**, 2689 (1997).
- [23] L. P. Rokhinson, D. C. Tsui, L. N. Pfeiffer, and K. W. West, *Superlattices Microstruct.* **32**, 99 (2002).
- [24] R. M. Potok, J. A. Folk, C. M. Marcus, and V. Umansky, *Phys. Rev. Lett.* **89**, 266602 (2002).
- [25] B. L. Altshuler, A. G. Aronov, A. I. Larkin, and D. E. Khmel'nitskii, *Zh. Eksp. Teor. Fiz.* **81**, 768 (1981) [*Sov. Phys. JETP* **54**, 411 (1981)].
- [26] Y. A. Bychkov and E. I. Rashba, *Pis'ma Zh. Eksp. Teor. Fiz.* **39**, 66 (1984) [*JETP Lett.* **39**, 78 (1984)].
- [27] H. L. Störmer, Z. Schlesinger, A. Chang, D. C. Tsui, A. C. Gossard, and W. Wiegmann, *Phys. Rev. Lett.* **51**, 126 (1983).
- [28] D. Stein, K. v. Klitzing, and G. Weimann, *Phys. Rev. Lett.* **51**, 130 (1983).
- [29] G. Usaj and C. A. Balseiro, *Phys. Rev. B* **70**, 041301(R) (2004).
- [30] S. Datta and B. Das, *Appl. Phys. Lett.* **56**, 665 (1990).
- [31] M. Khodas, A. Shekhter, and A. Finkelstein, *Phys. Rev. Lett.* **92**, 086602 (2004).